Growth of perturbations in dark energy parametrization scenarios

Ahmad Mehrabi
Department of Physics, Bu-Ali Sina University, Hamedan 65178, 016016, Iran

(Received 22 October 2017; published 27 April 2018)

In this paper, we study the evolution of dark matter perturbations in the linear regime by considering the possibility of dark energy perturbations. To do this, two popular parametrizations, Chevallier-Polarski-Linder (CPL) and Barboza-Alcaniz (BA), with the same number of free parameters and different redshift dependency have been considered. We integrate the full relativistic equations to obtain the growth of matter fluctuations for both clustering and smooth versions of CPL and BA dark energy. The growth rate is larger (smaller) than the ΛCDM in the smooth cases when $w < -1$ ($w > -1$), but the dark energy clustering gives a larger (smaller) growth index when $w > -1$ ($w < -1$). We measure the relative difference of the growth rate with respect to concordance ΛCDM and study how it changes depending on the free parameters. Furthermore, it is found that the difference of growth rates between smooth CPL and BA is negligible, less than 0.5%, while for the clustering case, the difference is considerable and might be as large as 2%. Eventually, using the latest geometrical and growth rate observational data, we perform an overall likelihood analysis and show that both smooth and clustering cases of CPL and BA parametrizations are consistent with observations. In particular, we find the dark energy figure of merit is approximately 70 for the BA and approximately 30 for the CPL, which indicates the BA model constrains relatively better than the CPL one.

DOI: 10.1103/PhysRevD.97.083522

I. INTRODUCTION

Dark energy (DE) is one of the fabulous concepts in modern cosmology introduced to explain the current acceleration expansion of Universe. Several distinct and independent observations including type-I supernovae [1–4], the cosmic microwave background (CMB) [5–9], baryon acoustic oscillation (BAO) [10–12], and large scale structures (LSS) [13–15] indicate that the current expansion of the Universe is accelerated. We know that, in the framework of General Relativity (GR), the gravitational force of ordinary matter pushes everything together. So, the current accelerating expansion of Universe requires an unusual component with negative pressure to overcome the gravity. On the other hand, one can assume the modification of gravity on large scales beyond GR to interpret the cosmic acceleration. The earliest and simplest candidate for DE is the cosmological constant (Λ), which has a negative pressure exactly equal to its energy density ($w_\Lambda = \frac{p_\Lambda}{\rho_\Lambda} = -1$) [16–18]. Such a component has no evolution during the cosmic history ($\rho_\Lambda = cte$) and miraculously dominates at recent time (coincidence problem). The cosmological constant acts like a vacuum energy, and by considering the cold dark matter as another component, one can make a cosmological model the so-called ΛCDM, which is highly consistent with current observations. However, the ΛCDM model suffers from severe theoretical fine-tuning and cosmic coincidence problems (see, for example, Refs. [18–23]).

As we mentioned above, modification of gravity is one solution to explain the current observations. In this approach, the laws of gravity change so that the accelerating expansion of Universe is realized without any DE fluid. In this way, the simplest possibility is the modification of Einstein-Hilbert action, which is proportional to the scalar curvature (R), and considering a generic function $f(R)$ instead [24–28]. The original form of such models suffers a strong instability [29], so people introduce more generalized models to avoid the problem. In addition to $f(R)$ gravity, there are other alternatives including scalar-tensor theories, Gauss-Bonnet gravity, and braneworld models, which can explain the current observations [30]. Generally, the modification of Einstein gravity leads to additional degrees of freedom, and if these come from higher derivatives, the theory suffers from Ostrogradsky ghost instability [31].

On the other hand, in the framework of GR, we need a fluid with negative pressure to explain current observations. To alleviate the theoretical problems appearing in ΛCDM theory, we can consider a cosmic fluid with $w \neq -1$. Based on the continuity equation for such a DE fluid, the energy density has an evolution during cosmic history and might alleviate the concordance problem. In addition, the DE fluid can be described by a scalar field in two different approaches: 1) a scalar field with a canonical Lagrangian, so-called quintessence models [32,33], and 2) a scalar field with a noncanonical Lagrangian, the so-called k-essence models, in which the negative pressure comes from the kinetic term [32,34–37].

DE not only accelerates the cosmic expansion but also affects the evolution of cosmic structures. It is well known that the galaxies and clusters of galaxy that we observe toady are developed from the initial fluctuations at the inflation era [38,39]. During the cosmic history, gravity can amplify the amplitude of these fluctuations, in particular at the matter-dominated epoch. Notice that at the DE-dominated phase DE suppresses the fluctuations and slows down the growth rate of structures. Two main properties of DE, which are needed to study the scenario of cosmological perturbations, are the equation-of-state (EoS) parameter $w_{\rm de}$ and the effective sound speed $c_e^2 = \frac{\delta p}{\delta \rho}$. Notice that at the background level the EoS parameter can solely describe the evolution of DE. However, at the perturbation level where we study the growth of fluctuations, the properties of DE are determined by both the EoS and effective sound speed parameters.

Two extreme cases have been extensively studied in the literature (see the following text for relevant references):

(i) Models with negligible effective sound speed, $c_e^2 \approx 0$. In this case, DE collapses like dark matter (DM) on sub-Hubble scales but with much smaller amplitude.

(ii) Models with an effective sound speed roughly equal to unity $c_e^2 \approx 1$ (in units of light speed $c = 1$). In this case, DE perturbations cannot grow on sub-Hubble scales.

More deeply speaking, we know that LSS data provide valuable information regarding the nature of DE [14,40]. DE changes the rate of growth, and measuring it on large scale structures through redshift space distortion can be used to understand the nature of DE. For scalar-based DE models such as quintessence models, the effective sound speed $c_e^2 \approx 1$, so DE is smooth on Hubble and smaller scales. On the other hand, in the k-essence models, c_e^2 can be negligible, and so DE perturbations grow through cosmic history [32,34,41–43]. The possibility of DE clustering and its effects on DM perturbations has been studied in several papers [44–56]. Specifically, the authors of Ref. [47] showed that CMB and LSS slightly prefer a dynamical DE with speed of sound differing from unity. On the other hand, the authors of Ref. [57] investigated the concentration parameter of massive galaxy clusters and pointed out that smooth DE is not very consistent with observations. Furthermore, the effects of negligible DE sound speed on the growth of DM perturbations in the GR framework are studied in Ref. [58], and it is revealed that $c_e^2 \approx 0$ is favored by observations.

In this work, we focus on the parametrization method to investigate the rule of EoS parameter $w_{\rm de}$ of DE on the scenario of cosmological structure formation. In the literature, one can find many different EoS parametrizations. One of the simplest and earliest parametrizations introduced by Chevallier-Polarski-Linder is the so-called CPL parametrization [59,60]. The CPL parametrization is the Taylor expansion of $w_{\rm de}$ with respect to the scale factor a up to first order as $w_{\rm de}(a) = w_0 + w_1(1-a)$ and consequently in terms of redshift as $w_{\rm de}(a) = w_0 + w_1 \frac{z}{1+z}$. Notice that, although the CPL is a well-behaved parametrization at early ($z \to \infty$) and present ($z = 0$) epochs, it diverges at future time ($z = -1$). Beside CPL parametrization, some purely phenomenological parametrizations have been proposed (see Ref. [61] for more details). The DE clustering scenarios mostly have been studied in w = cte(constant) + cold dark matter (wCDM) and CPL parametrizations in the literature, but it is not clear how DE clustering affects DM perturbations in different parametrizations, specifically when the evolution of the EoS parameter is different from the CPL. To address this, we investigate the phenomenological parametrization $w(z) = w_0 + w_1 \frac{z(1+z)}{1+z^2}$ introduced in Ref. [62] and hereafter called BA. The BA model provides a different redshift dependency, and through it, we can study how effects of DE clustering may change by different parametrizations. There are many available parametrizations that can be used in the current study, but we select the BA parametrization for two reasons: first, it has the same number of free parameters, so it is possible to study the effect of redshift dependency of the EoS, and second, it does not diverge at future times. In this paper, we examine how the DE clustering affects the growth rate of DM perturbations in these two parametrizations. Moreover, we study the BA parametrization as a rival model for the CPL in the scenario of cosmological structure formation and use the latest geometrical and growth rate data to examine the ability of these parametrizations against observations.

The structure of this paper is as follows. In Sec. II, we present the basic equations governing the evolution of the DE and DM at background and linear perturbation level. In Sec. III, the observational data sets are presented, and details of data processing are discussed. Finally, in Sec. IV, we conclude and discuss our results.

II. EVOLUTION OF DE AND DM

In this section, we first investigate the evolution of background cosmology and then study the growth of perturbations considering the CPL and BA DE models. To do these within GR, we need the Einstein field equations along with the continuity equations. We assume no direct interaction between DM and DE, and therefore each fluid evolves independently.

A. Background level

In the flat Friedmann-Robertson-Walker (FRW) Universe, the evolution of the Hubble parameter is given by

$$H^2 = H_0^2(\Omega_{dm}(z) + \Omega_{de}(z) + \Omega_{rd}(z)), \qquad (1)$$

where dm, de, and rd stand for DM, DE, and radiation, respectively, and $\Omega_x(z)$ presents the density parameter. It is

convenient to introduce the normalized Hubble parameter $E(z) = \frac{H(z)}{H_0}$, where H_0 is the present time Hubble parameter. In the case of noninteracting cosmic fluids, the continuity equation leads to $\Omega_{dm}(z) = \Omega_{dm}^{(0)}(1+z)^3$ for DM ($w = 0$), $\Omega_{rd}(z) = \Omega_{rd}^{(0)}(1+z)^4$ for radiation ($w = \frac{1}{3}$) and

$$\Omega_{de}(z) = \Omega_{de}^{(0)}(1+z)^3 \exp \int_0^z \frac{w(z)}{1+z} dz \tag{2}$$

for a DE fluid with an arbitrary EoS parameter. The superscript (0) indicates the present time value of quantities. Notice that in a flat Universe $\Omega_{rd}^{(0)} + \Omega_{dm}^{(0)} + \Omega_{de}^{(0)} = 1$, and hereafter, we confine ourself to a flat Universe. Now, we calculate the energy density of DE for the two CPL and BA parametrizations considered in this work. The EoS parameter of CPL in terms of redshift is given by

$$w_{\mathrm{CPL}}(z) = w_0 + w_1 \frac{z}{1+z}, \tag{3}$$

where w_0 and w_1 are two free parameters of the model. Using the continuity equation, the density parameter in this case is

$$\Omega_{de}(z) = \Omega_{de}^{(0)}(1+z)^{3(1+w_0+w_1)} \exp \frac{-3w_1 z}{1+z}. \tag{4}$$

The EoS parameter of BA reads

$$w_{\mathrm{BA}}(z) = w_0 + w_1 \frac{z(1+z)}{1+z^2}, \tag{5}$$

with two free parameters like the CPL model. Here, the energy density of DE can be easily obtained. In this case, the density parameter is

$$\Omega_{de}(z) = \Omega_{de}^{(0)}(1+z)^{3(1+w_0)}(1+z^2)^{\frac{3}{2}w_1}. \tag{6}$$

At present and early times, these two parametrizations are the same, but at the far future $z \to -1$, the CPL diverges, while the BA gives a constant value. These two models differ from each other due to different redshift dependencies. We show the difference between the two parametrizations, $w_{\mathrm{BA}} - w_{\mathrm{CPL}}$, in units of w_1 in Fig. 1, which indicates a maximum difference of around 0.55 at redshift $z \sim 2$. Such a difference in the EoS affects not only the Hubble parameter but also the growth of rate of perturbations. To realize how various redshift dependencies affect the Hubble parameter as well as growth of perturbations, we measure the relative difference of these two quantities in this and subsequent parts. The relative difference between the Hubble parameter with respect to the concordance ΛCDM one is computed as

$$\Delta E(\%) = \frac{E_{\mathrm{CPL,BA}} - E_{\Lambda\mathrm{CDM}}}{E_{\Lambda\mathrm{CDM}}} \times 100, \tag{7}$$

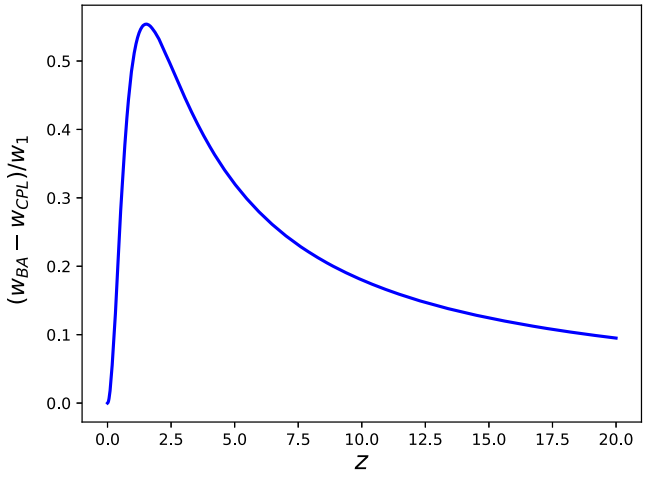

FIG. 1. The relative difference of EoS of our models in units of w_1 with respect to the cosmic redshift.

where E_Λ is the Hubble parameter for the ΛCDM. In Fig. 2, we show the evolution of the relative difference ΔE as a function of redshift z for different values of free parameters w_0 and w_1. Here, for all cases, we fix w_0 to -0.9 and allow that w_1 gets -0.2 and $+0.2$, only to show how these two models affect the Hubble parameter.

As expected, at the present time, all cases coincide with each other because of the normalization of the Hubble parameter. We observe that the difference between different parametrizations occurs at low redshifts between $z \sim 1$ and 2. This result is so interesting since at low redshifts DE dominates the total energy of Universe and the dynamics of the whole Universe is determined by DE. In the case of $w_1 = -0.2$, we observe that for both CPL and BA the quantity ΔE is roughly 1% at redshift around $z \sim 1.7$, while in the case of $w_1 = 0.2$, this value is approximately 5%-6%

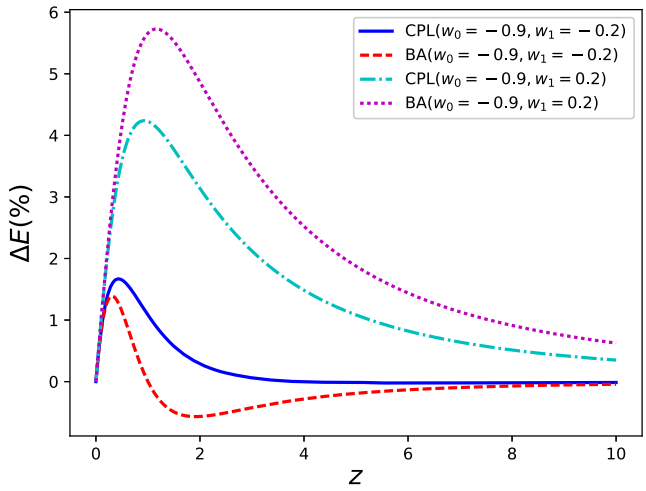

FIG. 2. The redshift evolution of percentage relative difference between Hubble parameters of CPL and BA parametrizations with respect to the standard ΛCDM model.

at $z \sim 1.6$. We also observe that in the case of $w_1 = 0.2$ the maximum of ΔE for BA parametrization is roughly 2% larger than the CPL one. Moreover, for $w_1 = -0.2$ ($w_1 = 0.2$), the BA parametrization results are smaller (larger) ΔE compared to CPL. At high redshifts, we see that the difference goes to zero for all parameters. This means that at early times (DM-dominated epoch) the effect of DE on the dynamics of the Universe is negligible. The Hubble parameter not only affects the evolution of cosmic fluid but also has a direct influence on the evolution of fluctuations. We will see in the next subsection how the Hubble parameter difference alters the growth of fluctuations.

B. Perturbation level

In the framework of GR, the evolution of perturbations can be described using the conformal Newtonian gauge. In this gauge, the perturbed FRW metric is given by

$$ds^2 = a(t)^2[(1+2\psi)d\eta^2 - (1-2\phi)\delta_{ij}dx^i dx^j], \quad (8)$$

where ψ and ϕ are the Bardeen potentials and η is the conformal time. For a fluid without anisotropic stress, the Einstein equations imply $\psi = \phi$, but for modified gravity models, this is not true generally. In the following, we assume the DE fluid has no anisotropic stress so these two potentials are the same. The Einstein equations in the perturbed FRW metric read

$$3\mathcal{H}\phi' + (3\mathcal{H}^2 + k^2)\phi = -\frac{3\mathcal{H}^2}{2}(\Omega_{\rm m}\delta_{\rm m} + \Omega_{\rm d}\delta_{\rm d}), \quad (9)$$

$$\phi'' + 3\mathcal{H}\phi' + \left(\frac{2a''}{a} - \mathcal{H}^2\right)\phi = \frac{3\mathcal{H}^2}{2}\Omega_{\rm d}\frac{\delta p_{\rm d}}{\delta\rho_{\rm d}}\delta_{\rm d}, \quad (10)$$

where $\mathcal{H} = aH$ is the conformal Hubble parameter and the prime denotes a derivative with respect to the conformal time. Here, δ_m and δ_d are the perturbations of DM and DE, respectively. Notice that in Eqs. (9) and (10) we consider a general case in which both DM and DE have been perturbed. For subhorizon scales $\mathcal{H}^2 \ll k^2$ and in the matter-domination epoch $\phi \approx cte$, the first equation turns to the usual Poisson equation,

$$k^2\phi = -\frac{3\mathcal{H}^2}{2}(\Omega_{\rm m}\delta_{\rm m} + \Omega_{\rm d}\delta_{\rm d}). \quad (11)$$

The continuity equations at the perturbation level for a general fluid are [63]

$$\delta_i' = -(1+w_i)(\theta_i - 3\phi') - 3\frac{a'}{a}\left(\frac{\delta p_i}{\delta\rho_i} - w_i\right)\delta_i, \quad (12)$$

$$\theta_i' = -\frac{a'}{a}(1-3w_i)\theta_i - \frac{w_i'}{1+w_i}\theta_i + \frac{\frac{\delta p_i}{\delta\rho_i}}{1+w_i}k^2\delta + k^2\phi, \quad (13)$$

where θ is the divergence of velocity. The ratio of pressure to density perturbation $\frac{\delta p_i}{\delta\rho_i}$ needs to be a gauge-invariant quantity, so it is given by [44]

$$\frac{\delta p}{\delta\rho} = c_{\rm e}^2 + 3\mathcal{H}(1+w)(c_{\rm e}^2 - c_{\rm a}^2)\frac{\theta}{\delta}\frac{1}{k^2}, \quad (14)$$

where c_e^2 and c_a^2 indicate the effective and adiabatic sound speed squared, respectively. The adiabatic sound speed squared is given by

$$c_{\rm a}^2 = w - \frac{a\frac{dw}{da}}{3(1+w)}, \quad (15)$$

which is determined by the EoS parameter and so is negative for most of the DE models. The negative value of sound speed squared ($c_{\rm a}^2 < 0$) leads to unstable exponential growth of perturbations. Fortunately, the pressure perturbation is given in terms of the effective sound speed and not the adiabatic one, and the problem can be avoided when we deal with the effective sound speed. In contrast to the adiabatic sound speed, the effective sound speed squared is a positive value in the range of [0, 1] (for more details about DE sound speed, see the next subsection). Here, we assume both smooth ($c_e \sim 1$) and clustered ($c_e \sim 0$) DE scenarios and study their effects on the growth of matter perturbations within the framework of DE parametrizations considered in this work.

Taking another derivative of Eq. (12) and using Eqs. (9) and (13), we can obtain a second-order differential equation that governs the evolution of perturbations for the fluids [58]. These differential equations are in the forms

$$\frac{d^2\delta_{\rm m}}{da^2} + \frac{1}{a}\left(2 + \frac{\mathcal{H}'}{\mathcal{H}^2}\right)\frac{d\delta_{\rm m}}{da} = S, \quad (16)$$

$$\frac{d^2\delta_{\rm d}}{da^2} + \frac{1}{a}\left[2 + \frac{\mathcal{H}'}{\mathcal{H}^2} + 3c_{\rm a}^2 - 6w_{\rm d}\right]\frac{d\delta_{\rm d}}{da} + B_d\delta_{\rm d} = (1+w_{\rm d})S, \quad (17)$$

where B_d and S are given by

$$B_{\rm d} = \frac{1}{a^2}\left[3(c_{\rm e}^2 - w_{\rm d})\left(1 + \frac{\mathcal{H}'}{\mathcal{H}^2} - 3w_{\rm d} + 3c_{\rm a}^2 - 3c_{\rm e}^2\right) + \frac{k^2}{\mathcal{H}^2}c_{\rm e}^2 - 3a\frac{dw_{\rm d}}{da}\right],$$
$$S = \frac{3\mathcal{H}^2}{2}(\Omega_{\rm m}\delta_{\rm m} + \Omega_{\rm d}\delta_{\rm d}). \quad (18)$$

To obtain the DE perturbation equation, we set $c_e^2 = 0$ and substitute Eq. (14) into Eqs. (12) and (13), but in the case of smooth DE, we set $\delta_d = 0$ in these equations. Notice that the source term in Eq. (17) is proportional to $1 + w_{\rm d}$, so any

DE perturbation vanishes in the case of standard ΛCDM cosmology. In Eqs. (16) and (17), we need to know the derivative of the Hubble parameter that can be easily obtained from the Friedman equations as follows:

$$\frac{\mathcal{H}'}{\mathcal{H}^2} = -\frac{1}{2}(1 + 3\Omega_{\rm d} w_{\rm d}). \tag{19}$$

To solve the perturbation equations (16) and (17), we use the initial conditions [58,64]

$$\delta_{\rm m,i} = -2\phi_{\rm i}\left(1 + \frac{k^2}{3\mathcal{H}_{\rm i}^2}\right), \tag{20}$$

$$\frac{d\delta{\rm m,_i}}{da} = -\frac{2}{3}\frac{k^2}{\mathcal{H}_{\rm i}^2}\phi_{\rm i}, \tag{21}$$

$$\delta_{\rm d,i} = (1 + w_{\rm d})\delta_{\rm m,i}, \tag{22}$$

$$\frac{d\delta_{\rm d,i}}{da} = (1 + w_{\rm d})\frac{d\delta_{\rm m,i}}{da} + \frac{dw_{\rm d}}{da}\delta_{\rm m,i}, \tag{23}$$

where we set $\phi_i = -6 \times 10^{-7}$. These initial conditions lead to a linear perturbation ($\delta_m \approx 0.1$) for scale $k = 0.15h$ Mpc^{-1}. In this work, we fix the scale to $k = 0.15h$ Mpc^{-1} and integrate the perturbation equations numerically from $a = 0.01$ to the present time. We should note that varying the value of k to other linear scales has a very tiny effect on the evolution of perturbations, as discussed in Ref. [58]. Furthermore, notice that the initial conditions for DE perturbations are given by assuming an adiabatic condition [37,65].

To compare our results with observation, the relevant quantity is the product of growth rate f and mass variance in a sphere of radius 8 Mpc/h (σ_8). The growth rate at any redshift is given by

$$f(z) = -\frac{1+z}{\delta_m(z)}\frac{d\delta_m(z)}{dz}. \tag{24}$$

Also, the mass variance at a given redshift is $\sigma_8(z) = \sigma_8 \frac{\delta_m(z)}{\delta_m(z=0)}$, where σ_8 is the mass variance at the present time. Generally, the mass variance at the present time is a free parameter and can be constrained using the observational data.

To realize how DE perturbations affect the growth of DM perturbations, we fix $\Omega_m = 0.3$, $h = 0.7$ and compute the relative difference of $f\sigma_8(z)$ for CPL and BA parametrizations with that of in the ΛCDM according the following relation:

$$\Delta f\sigma_8 = \frac{f\sigma_{8,\rm model} - f\sigma_{8,\Lambda}}{f\sigma_{8,\Lambda}} \times 100. \tag{25}$$

Since our parametrizations have two free parameters, we fix one parameter and present $\Delta f\sigma_8$ as a function of the other parameter. In Fig. 3, we set $w_1 = 0.2$ and show the evolution of $\Delta f\sigma_8$ calculated at the present time as a function of w_0 for both smooth and clustering DE scenarios. The results for smooth CPL and BA are very close to each other, and the differences are less than 0.5%. However, for clustered CPL and BA cases, the difference is relatively large, and we measure it as $0.5\% - 2.5\%$ for w_0 in the range $(-1.3, -0.7)$.

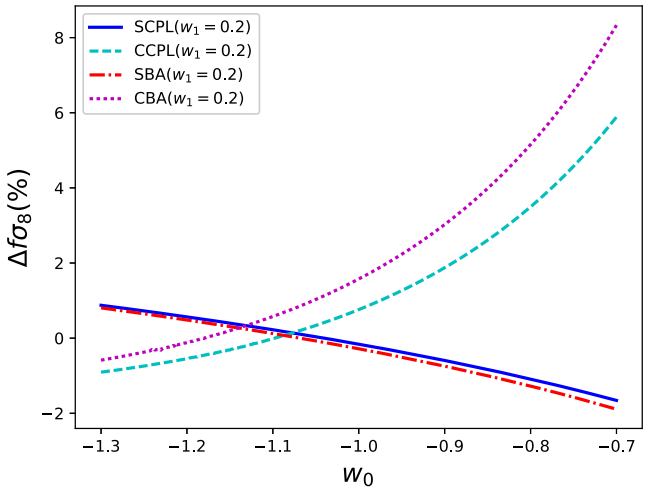

FIG. 3. The relative growth rate as a function of w_0 for the CPL and BA parametrizations. SCPL and SBA (CCPL and CBA) indicate smooth CPL and BA (clustered CPL and BA) models.

Moreover, the smooth and clustered DE behave differently on both sides of $w_{\rm d} = -1$. We observe that $\Delta f\sigma_8$ is positive for clustering cases when $w_{\rm d} > -1$ and may reach to 8% for $w_0 = -0.7$. On the other hand, the relative growth rate is negative for smooth DE parametrizations when $w_{\rm d} > -1$, but the differences with respect to the ΛCDM model are around 2% for $w_0 = -0.7$. In addition, one can measure the small difference between smooth and clustering cases when the EoS parameter crosses the phantom line ($w_{\rm d} < -1$). The different behaviors of clustered DE models on both sides of phantom line ($w_{\rm d} = -1$) can be described as follows. When the EoS of DE crosses the phantom line, the sign of the source term in Eq. (17) changes, and DE perturbations are negative and vise versa.

Another interesting point that might be realized from Fig. 3 is that for DE in the regime $w_{\rm d} > -1$ ($w_{\rm d} < -1$) the growth rate of DM perturbations is larger (smaller) compared to the ΛCDM. This prediction can be easily understood from an extra term due to DE perturbations (δ_d) in the source term of the DM perturbation equation, which is positive (negative) in the case $w_{\rm d} > -1$ ($w_{\rm d} < -1$). For smooth DE models, there is no δ_d, and the growth of DM perturbations is affected by the evolution of the Hubble parameter. As is clear from Fig. 2, the Hubble quantity is larger than the ΛCDM for the $w_{\rm d} > -1$ regime, so the growth rate is smaller.

In Fig. 4, we show the evolution of $\Delta f\sigma_8(z = 0)$ as a function of w_1 where w_0 is fixed to -0.9. We observe that the evolution of $\Delta f\sigma_8(z = 0)$ with respect to w_1 is similar to the previous one. However, our result shows a very small difference for smooth DE models (less than 0.5%) when w_1

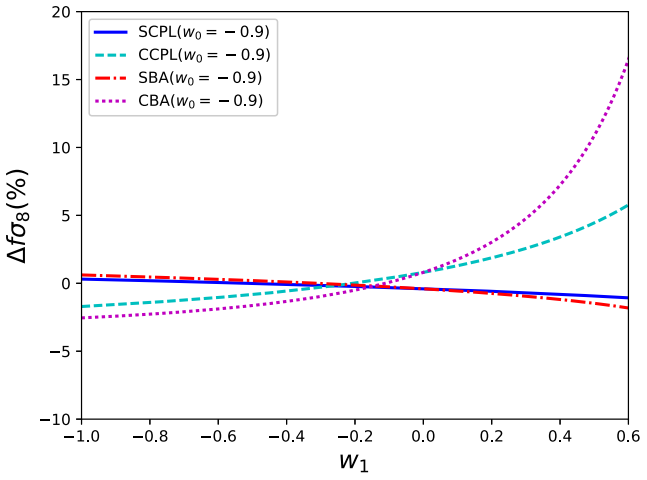

FIG. 4. The relative growth rate as a function of w_1 for the CPL and BA parametrizations. SCPL and SBA (CCPL and CBA) indicate smooth CPL and BA (clustered CPL and BA) models.

is in the range $(-1, 0.6)$. For clustered DE models, when $w_1 < 0$, the difference is small, but for a positive value of w_1, the difference is relatively larger and might be as large as 10% for $w_1 = 0.6$. Furthermore, the result shows a tiny difference between our models and the ΛCDM for $w_1 < 0$ in both cases of smooth and clustering DE. For $w_1 > 0$, the smooth DE does not change the growth rate significantly compared to the ΛCDM, but for the clustering case, the difference increases rapidly as w_1 increases and might be as large as 17% for $w_1 = 0.6$.

From the above statements, it has been revealed how the EoS parameter of DE affects the DM growth rate in both the smooth and clustering DE cases. For smooth DE, these two parametrizations roughly give similar results, but in the latter case, the growth rate might considerably be different in these two models, which is due to the different redshift dependencies. Based on our analysis, various redshift dependencies of EoS might change the growth rate around 2% in clustering DE scenarios, which is four times larger than the growth rate difference in the smooth DE. Using current observational data, it is not possible to distinguish between smooth and clustering DE cases, but according to Refs. [66,67], a combination of weak lensing and the peculiar velocity observations can break the degeneracy of the DE clustering (no anisotropic stress) and some modified gravity theories and also distinguish between the smooth and clustering DE cases. So, further cosmological data, for example, data from Euclid, can improve the quality of data, and it might be possible to distinguish between clustering or smooth DE.

C. DE sound speed

Since the DE sound speed is a crucial quantity in the clustering DE, it is worth it to discuss it with more details. In a general case, the pressure not only depends on the energy density but also on the entropy s, so $p(\rho, s)$ and its perturbation are

$$\delta p = \left(\frac{\partial p}{\partial \rho}\right)_s \delta\rho + \left(\frac{\partial p}{\partial s}\right)_\rho \delta s, \tag{26}$$

where $(\frac{\partial p}{\partial \rho})_s$ is the adiabatic sound speed squared and the second term is due to entropy perturbation [68]. Hence, we have

$$\frac{\delta p}{\delta \rho} = c_a^2 + \left(\frac{\partial p}{\partial s}\right)_\rho \frac{\delta s}{\delta \rho}. \tag{27}$$

For a perfect fluid, there is no entropy perturbation, and the second term vanishes. In this case, the pressure perturbation is given in terms of the adiabatic sound speed squared, and it is negative for most DE models. However, the second term can compensate the first, and the pressure perturbation become zero or positive. The sum of these two terms results in the effective sound speed of the DE, which is the related quantity in the case of DE perturbations.

As we mentioned, it is generally believed that if the sound speed squared for a fluid is negative, its perturbations are unstable. However, by considering the perturbation of entropy, the problem can be avoided. The second term in Eq. (26) can be dominated due to some dissipative process, and consequently, it would change the effective sound speed of DE to a null or positive value [68]. Notice that the above discussion is important when we consider the clustering DE models. In the cases of smooth DE scenarios, we need only the EoS parameter of DE to determine the evolution of DM perturbations.

III. OBSERVATIONAL DATA AND LIKELIHOOD ANALYSIS

To check the validity of our models with observational data, we perform a Markov chain Monte Carlo (MCMC) analysis using the most recent data. Basically, the observational data consist of two parts: 1) data to constrain the background parameters and 2) data to constrain the growth rate of DM perturbations (at the first level). We use the most recent SN Ia (JLA sample), BAO, CMB, and Hubble parameter data to constrain the background parameters including (Ω_m, h, w_0, w_1) and also the growth rate of perturbations, $f\sigma_8$ data, to constrain our models at the first perturbation level. In the following, we first briefly explain the data set and then the procedure of the MCMC

TABLE I. The BAO data used in this work.

z	d_i	Survey and references
0.106	0.336	6dF [72]
0.35	0.113	SDSS-DR7 [73]
0.57	0.073	SDSS-DR9 [74]
0.44	0.0916	WiggleZ [12]
0.6	0.0726	WiggleZ [12]
0.73	0.0592	WiggleZ [12]

TABLE II. The best values of parameters and the 1σ uncertainties for the smooth case.

Parameter	CPL	BA
Ω_m	$0.281\,5 \pm 0.0073$	$0.282\,3 \pm 0.0076$
h	$0.696\,5 \pm 0.0056$	$0.695\,7 \pm 0.0055$
w_0	-0.896 ± 0.079	-0.908 ± 0.069
w_1	$-0.50^{+0.41}_{-0.35}$	$-0.27^{+0.23}_{-0.17}$
σ_8	0.754 ± 0.018	0.753 ± 0.018

TABLE III. The best values of parameters and the 1σ uncertainties for the clustering case.

Parameter	CPL	BA
Ω_m	$0.281\,4 \pm 0.0078$	$0.281\,9 \pm 0.0073$
h	$0.696\,4 \pm 0.0057$	0.6963 ± 0.0053
w_0	$-0.900^{+0.079}_{-0.091}$	-0.912 ± 0.065
w_1	$-0.48^{+0.44}_{-0.36}$	$-0.26^{+0.21}_{-0.18}$
σ_8	0.757 ± 0.017	0.757 ± 0.017

analysis. Finally, we present the best value of the parameters as well as their uncertainties and discuss the results.

For the JLA SN sample, the theoretical value of distance module μ_{th} is given by

$$\mu_{th} = 5\log_{10}\left(\frac{d_L(z_{hel}, z_{cmb})}{\text{Mpc}}\right) + 25, \tag{28}$$

where d_L is the luminosity distance and z_{cmb} (z_{hel}) is the CMB rest-frame (heliocentric) redshift of SN. The luminosity distance d_L is given by [69]

$$d_L = (1 + z_{hel})r(z_{cmb}), \tag{29}$$

where $r(z)$ is the comoving distance that is given in terms of the normalized Hubble parameter. The observational distance module is given by the empirical relation [70]

$$\mu_{\text{obs}} = m_B - M_B + \alpha \times \mathbf{x_1} - \beta \times \mathbf{C}, \tag{30}$$

where m_B corresponds to the observed peak magnitude in rest frame of the B band and α, β, and M_B are nuisance

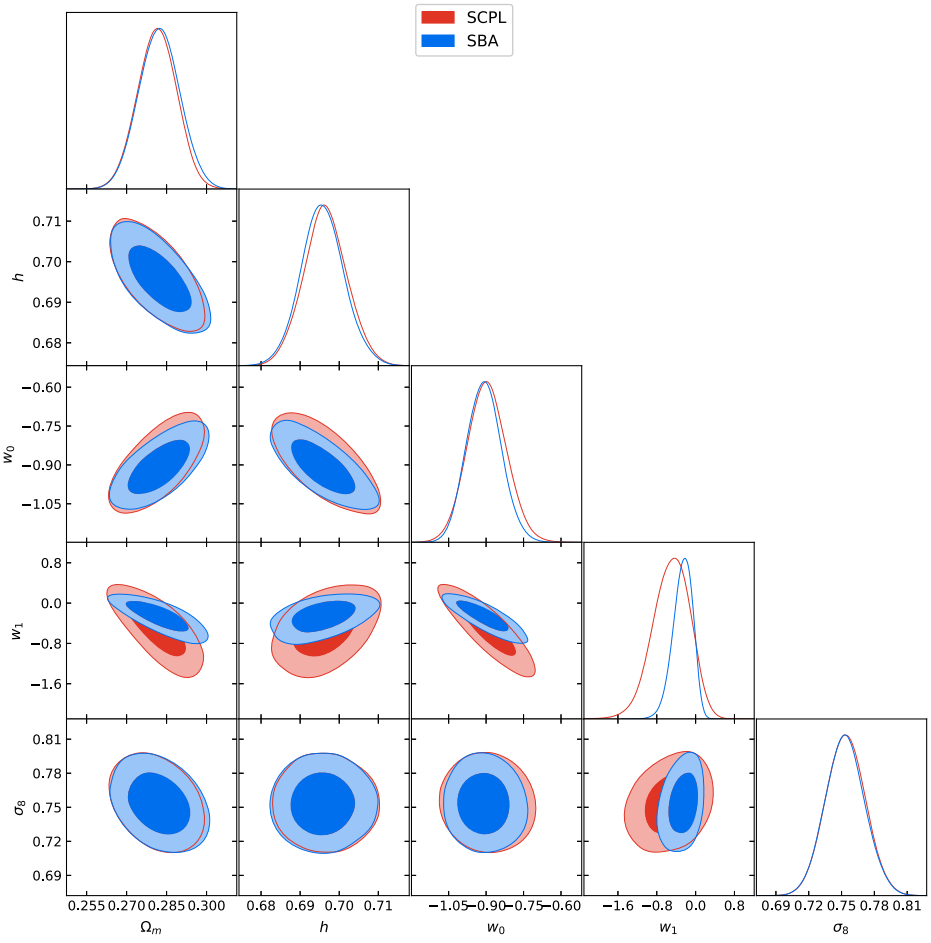

FIG. 5. The confidence regions for smooth DE.

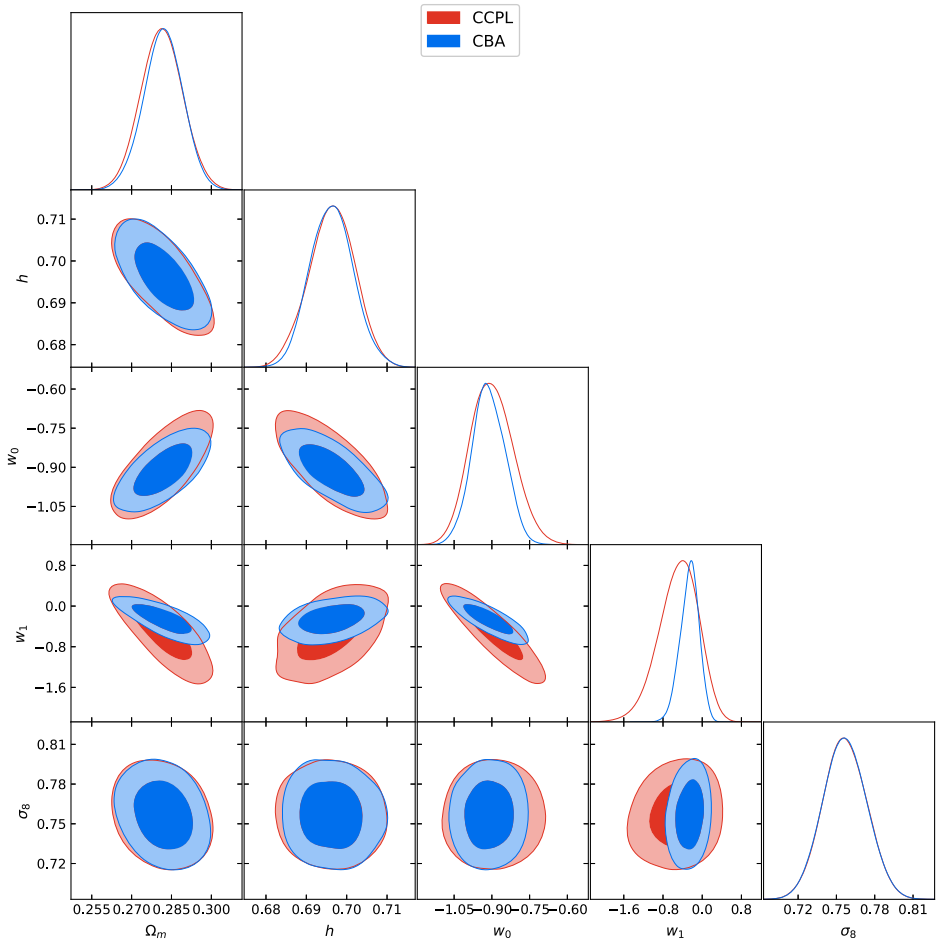

FIG. 6. The confidence regions for clustering DE.

parameters that should be marginalized at the end. To see details and the definition of other parameters, see Ref. [70]. The χ^2 of SN data is given by

$$\chi^2_{sn} = \Delta\mu^T \mathbf{Cov}^{-1}_{sn} \Delta\mu, \tag{31}$$

where $\Delta\mu = \mu_{\rm obs} - \mu_{th}$ and $\mathbf{Cov}_{sn}$ is the total covariance matrix that includes statistical and systematic uncertainties (for more details of the covariance matrix, see Ref. [70]).

The next data set is the BAO, which is based on the observed baryon oscillations in the power spectrum of the galaxy correlation function. In our analysis, we use six distinct data points, which are presented in Table I. In this case, the quantity $\chi^2_{\rm bao}$ in terms of the covariance matrix is given by

$$\chi^2_{\rm bao} = \mathbf{Y}^T \mathbf{C}^{-1}_{\rm bao} \mathbf{Y}, \tag{32}$$

where we use $\mathbf{Y}$ and $\mathbf{C}_{\rm bao}$ from Ref. [71].

Since the position of the CMB acoustic peaks depends on the DE dynamics through the angular diameter distance, the CMB data provide valuable information to constrain a DE model. The process of calculating χ^2_{cmb} (for Planck data) is not repeated here, and we refer reader to Ref. [58] for more details.

Furthermore, we use an updated version of the Hubble parameter compared to our previous one in Ref. [58]. The Hubble parameter in this work is those data (38 data points) collected in Ref. [75]. For this data set, the χ^2 is given by

$$\chi^2_{\rm h} = \sum_i \frac{[H(z_i) - H_{\rm ob,i}]^2}{\sigma_i^2}, \tag{33}$$

where $H(z_i)$ $(H_{\rm ob,i})$ is the theoretical (observational) Hubble parameter.

In addition to the above data, we use the growth rate data $(f\sigma_8)$, which are obtained from redshift space distortion (RSD). Since not all of the current available data points are independent, we use data introduced in Ref. [76], which are an independent set of growth rate data.

Finally, since the overall likelihood is the product of each likelihood, the total χ^2 is given by

$$\chi^2_{\rm tot} = \chi^2_{\rm sn} + \chi^2_{\rm bao} + \chi^2_{\rm cmb} + \chi^2_H + \chi^2_{\rm fs}. \quad (34)$$

We use the MCMC method to find the best value of parameters as well as their uncertainties. The results are summarized in Tables II and III for the smooth and clustering cases, respectively. In addition, the 1σ and 2σ confidence regions of the free parameters are presented in Figs. 5 and 6.

Our results almost show the same confidence regions for the free parameters Ω_m, h, and σ_8. However, the DE parameters are constrained slightly differently, and interestingly, the area of confidence regions for the BA model is smaller than the CPL one for both the smooth and clustering cases. To quantify this, the DE figure of merit (FoM) is often defined as $\frac{1}{\Delta w_0 \Delta w_1}$, where Δw_0 and Δw_1 are uncertainties of the parameters at 1σ level. A large value of FoM means a better constraint, and our results indicate that the BA model provides a better constraint than the CPL in both the smooth and clustering cases. The FoM for BA parametrization is $\sim$70, while it is $\sim$30 for the CPL model (the difference for smooth and clustering cases is very small).

To check the consistency of our models with the observational data, the corrected Akaike Information Criterion (AIC) has been used. This quantity is given by

$$\mathrm{AIC} = \chi^2_{\rm min} + 2n_{\rm fit}, \quad (35)$$

where $n_{\rm fit}$ is number of the free parameters. To compare two models, the pair differences $\Delta\mathrm{AIC} = \mathrm{AIC}_y - \mathrm{AIC}_x$ have to be computed. Two models with $|\Delta\mathrm{AIC}| \leq 2$ are consistent, while $|\Delta\mathrm{AIC}| \geq 6$ indicates strong evidence against the model with larger AIC. In Table IV, the AIC values for the two parametrizations as well as the ΛCDM model are shown.

According to the AIC criterion, all models are consistent with the data, and there is no positive nor strong evidence against these models compared to ΛCDM. However, our results show the DE clustering provides a smaller AIC compared to the smooth cases, which indicates the data slightly prefer DE clustering, but of course it is not significant with current data. Notice that a similar conclusion is reported in Refs. [77–79], which indicates good agreement of our results with other works. As we mentioned above, the future observational data, for example, based on the Euclid, are expected to improve the quality of data significantly, and thus the validity of DE clustering will be tested in the near future.

TABLE IV. The AIC value for our models.

Model	AIC
SCPL	728.9
SBA	728.4
CCPL	727.8
CBA	727.1
ΛCDM	728.3

IV. CONCLUSION

To summarize, we studied the growth of matter perturbations by considering the possibility of DE perturbations. We considered CPL and BA parametrizations with an equal number of free parameters but different redshift dependencies and integrated the relativistic linear equations to realize the evolution of DM and DE perturbations. Since from previous works it was not clear how DE clustering affects the growth rate in different EoS parametrizations, we selected the BA model with a different redshift dependency to investigate and compare to the CPL as well as the ΛCDM. Moreover, in contrast to the CPL parametrization, the BA model gives a finite value at far future times ($z \to -1$). We obtained the relative difference of the Hubble parameter, which depends on the free parameters. For instance, for parameters $w_0 = -0.9, w_1 = 0.2$, the Hubble parameter of the BA (CPL) model is around 6% (4%) larger than the ΛCDM case. So, for the same values of free parameters, the Hubble parameter in these two models differs around $\sim$2% due to the different redshift dependencies.

We examined both the smooth and clustering DE cases within the framework of CPL and BA parametrizations and calculated the relative difference of the growth rate to show the effect of DE clustering on the scenario of structure formation in the Universe. The growth rate is larger (smaller) than ΛCDM in the smooth DE cosmology for $w < -1$ ($w > -1$). In contrast to this, DE clustering gives a larger (smaller) growth index for $w > -1$ ($w < -1$). We observed a (1–2)% difference between the parametrizations analyzed in this work and ΛCDM when we fixed $w_1 = 0.2$ and allowed w_0 to vary in range $(-1.3, -0.7)$ for smooth DE (1%–8% for clustered DE). We also examined how the growth rate changes with respect to the w_1 parameter, and it was found that the difference between our parametrizations and the concordance ΛCDM model is very small in the case of smooth DE. However, in the case of DE clustering, the difference might be as large as 17% (6%) when $w_0 = -0.9$ and $w_1 = 0.6$ for the BA (CPL) model. Notice that the difference between the growth rate of these parametrizations is due to the different redshift dependencies of the EoS, so our results indicate that in the case of clustered DE understanding the exact functional form of the EoS parameter is a crucial quantity but its effect is not significant in the case of smooth DE. A combination of weak lensing and the peculiar velocity observations can distinguish between the smooth or clustered DE [66,67].

To check the consistency of our models with observation, we used current available data including SN Ia (the JLA sample), Planck CMB, BAO, the Hubble parameter, and the growth rate $f\sigma_8$ to put constraints on the cosmological parameters. The MCMC method was used to obtain the best-fit values of the parameters as well as their uncertainties.

We obtained almost the same confidence regions for Ω_m, h, σ_8 pairs. However, this was not the case for the w_0, w_1 pair. We measured the FoM of DE as approximately 70 for the BA and approximately 30 for the CPL parametrizations with a tiny difference between the smooth and clustering cases. This means that, apart from the type of DE (smooth or clustering) scenarios, the BA parametrization provides a tighter constraint compared to the CPL. Hence, based on this result, we suggest the BA parametrization instead of the CPL as a totally better approximation for the EoS parameter. Finally, on the basis of the AIC criterion, these two parametrizations are consistent with observations as equally as the ΛCDM cosmology. As a comparison between clustering and smooth DE scenarios, we found a smaller AIC for clustering cases, which indicates that the observational data slightly prefer clustered DE models.

[1] S. Perlmutter *et al.* (Supernova Cosmology Project Collaboration), Astrophys. J. **483**, 565 (1997).
[2] S. Perlmutter *et al.* (Supernova Cosmology Project Collaboration), Nature (London) **391**, 51 (1998).
[3] S. Perlmutter *et al.* (Supernova Cosmology Project Collaboration), Astrophys. J. **517**, 565 (1999).
[4] A. G. Riess *et al.* (Supernova Search Team Collaboration), Astrophys. J. **607**, 665 (2004).
[5] C. Bennett *et al.* (WMAP Collaboration), Astrophys. J. Suppl. Ser. **148**, 1 (2003).
[6] D. Spergel *et al.* (WMAP Collaboration), Astrophys. J. Suppl. Ser. **148**, 175 (2003).
[7] D. Spergel *et al.* (WMAP Collaboration), Astrophys. J. Suppl. Ser. **170**, 377 (2007).
[8] Planck Collaboration XIII, Astron. Astrophys. **594**, A13 (2016).
[9] Planck Collaboration XIV, Astron. Astrophys. **594**, A14 (2016).
[10] D. J. Eisenstein *et al.* (SDSS Collaboration), Astrophys. J. **633**, 560 (2005).
[11] H.-J. Seo and D. J. Eisenstein, Astrophys. J. **633**, 575 (2005).
[12] C. Blake *et al.*, Mon. Not. R. Astron. Soc. **418**, 1707 (2011).
[13] E. Hawkins *et al.*, Mon. Not. R. Astron. Soc. **346**, 78 (2003).
[14] M. Tegmark *et al.* (SDSS Collaboration), Phys. Rev. D **69**, 103501 (2004).
[15] S. Cole *et al.* (2dFGRS Collaboration), Mon. Not. R. Astron. Soc. **362**, 505 (2005).
[16] S. Weinberg, Rev. Mod. Phys. **61**, 1 (1989).
[17] P. Peebles and B. Ratra, Rev. Mod. Phys. **75**, 559 (2003).
[18] V. Sahni and A. Starobinsky, Int. J. Mod. Phys. D **9**, 373 (2000).
[19] S. Weinberg, Rev. Mod. Phys. **61**, 1 (1989).
[20] S. M. Carroll, Living Rev. Relativity **4**, 1 (2001).
[21] P. J. Peebles and B. Ratra, Rev. Mod. Phys. **75**, 559 (2003).
[22] T. Padmanabhan, Phys. Rep. **380**, 235 (2003).
[23] E. J. Copeland, M. Sami, and S. Tsujikawa, Int. J. Mod. Phys. D **15**, 1753 (2006).
[24] H.-J. Schmidt, Astron. Nachr. **311**, 165 (1990).
[25] G. Magnano and L. M. Sokolowski, Phys. Rev. D **50**, 5039 (1994).
[26] A. Dobado and A. L. Maroto, Phys. Rev. D **52**, 1895 (1995).
[27] S. Capozziello, S. Carloni, and A. Troisi, Recent Res. Dev. Astron. Astrophys. **1**, 625 (2003).
[28] S. M. Carroll, V. Duvvuri, M. Trodden, and M. S. Turner, Phys. Rev. D **70**, 043528 (2004).
[29] A. D. Dolgov and M. Kawasaki, Phys. Lett. B **573**, 1 (2003).
[30] L. Amendola and S. Tsujikawa, *Dark Energy: Theory and Observations by Luca Amendola and Shinji Tsujikawa* (Cambridge University Press, Cambridge, England, 2010).
[31] R. P. Woodard, Lect. Notes Phys. **720**, 403 (2007).
[32] C. Armendariz-Picon, V. F. Mukhanov, and P. J. Steinhardt, Phys. Rev. Lett. **85**, 4438 (2000).
[33] E. J. Copeland, M. Sami, and S. Tsujikawa, Int. J. Mod. Phys. D **15**, 1753 (2006).
[34] C. Armendariz-Picon, T. Damour, and V. F. Mukhanov, Phys. Lett. B **458**, 209 (1999).
[35] T. Chiba, T. Okabe, and M. Yamaguchi, Phys. Rev. D **62**, 023511 (2000).
[36] T. Chiba, S. Dutta, and R. J. Scherrer, Phys. Rev. D **80**, 043517 (2009).
[37] L. Amendola and S. Tsujikawa, *Dark Energy: Theory and Observations* (Cambridge University Press, Cambridge, England, 2010).
[38] A. Linde, Phys. Lett. B **238**, 160 (1990).
[39] P. J. E. Peebles, *Principles of Physical Cosmology* (Princeton University, Princeton, NJ, 1993).
[40] M. Tegmark *et al.* (SDSS Collaboration), Phys. Rev. D **74**, 123507 (2006).
[41] J. Garriga and V. F. Mukhanov, Phys. Lett. B **458**, 219 (1999).
[42] E. Babichev, V. F. Mukhanov, and A. Vikman, J. High Energy Phys. 09 (2006) 061.
[43] R. Akhoury, D. Garfinkle, and R. Saotome, J. High Energy Phys. 04 (2011) 096.
[44] R. Bean and O. Doré, Phys. Rev. D **69**, 083503 (2004).
[45] W. Hu and R. Scranton, Phys. Rev. D **70**, 123002 (2004).
[46] G. Ballesteros and A. Riotto, Phys. Lett. B **668**, 171 (2008).
[47] R. de Putter, D. Huterer, and E. V. Linder, Phys. Rev. D **81**, 103513 (2010).
[48] D. Sapone and E. Majerotto, Phys. Rev. D **85**, 123529 (2012).
[49] R. Batista and F. Pace, J. Cosmol. Astropart. Phys. 06 (2013) 044.
[50] J. Dossett and M. Ishak, Phys. Rev. D **88**, 103008 (2013).
[51] T. Basse, O. E. Bjaelde, J. Hamann, S. Hannestad, and Y. Y. Wong, J. Cosmol. Astropart. Phys. 05 (2014) 021.
[52] R. C. Batista, Phys. Rev. D **89**, 123508 (2014).
[53] F. Pace, R. C. Batista, and A. Del Popolo, Mon. Not. R. Astron. Soc. **445**, 648 (2014).

[54] H. Steigerwald, J. Bel, and C. Marinoni, J. Cosmol. Astropart. Phys. 05 (2014) 042.
[55] A. Mehrabi, M. Malekjani, and F. Pace, Astrophys. Space Sci. **356**, 129 (2015).
[56] A. Mehrabi, S. Basilakos, M. Malekjani, and Z. Davari, Phys. Rev. D **92**, 123513 (2015).
[57] S. Basilakos, J. Bueno Sanchez, and L. Perivolaropoulos, Phys. Rev. D **80**, 043530 (2009).
[58] A. Mehrabi, S. Basilakos, and F. Pace, Mon. Not. R. Astron. Soc. **452**, 2930 (2015).
[59] M. Chevallier and D. Polarski, Int. J. Mod. Phys. D **10**, 213 (2001).
[60] E. V. Linder, Phys. Rev. Lett. **90**, 091301 (2003).
[61] M. Rezaei, M. Malekjani, S. Basilakos, A. Mehrabi, and D. F. Mota, Astrophys. J. **843**, 65 (2017).
[62] E. M. Barboza, Jr. and J. S. Alcaniz, Phys. Lett. B **666**, 415 (2008).
[63] C.-P. Ma and E. Bertschinger, Astrophys. J. **455**, 7 (1995).
[64] L. Abramo, R. Batista, L. Liberato, and R. Rosenfeld, Phys. Rev. D **79**, 023516 (2009).
[65] H. Kodama and M. Sasaki, Prog. Theor. Phys. Suppl. **78**, 1 (1984).
[66] Y.-S. Song, G.-B. Zhao, D. Bacon, K. Koyama, R. C. Nichol, and L. Pogosian, Phys. Rev. D **84**, 083523 (2011).
[67] S. Asaba, C. Hikage, K. Koyama, G.-B. Zhao, A. Hojjati, and L. Pogosian, J. Cosmol. Astropart. Phys. 08 (2013) 029.
[68] V. Mukhanov, *Physical Foundations of Cosmology* (Cambridge University Press, Cambridge, England, 2005), p. 442.
[69] S. Wang, S. Wen, and M. Li, J. Cosmol. Astropart. Phys. 03 (2017) 037.
[70] M. Betoule *et al.* (SDSS Collaboration), Astron. Astrophys. **568**, A22 (2014).
[71] G. Hinshaw *et al.* (WMAP Collaboration), Astrophys. J. Suppl. Ser. **208**, 19 (2013).
[72] F. Beutler, C. Blake, M. Colless, D. H. Jones, L. Staveley-Smith, L. Campbell, Q. Parker, W. Saunders, and F. Watson, Mon. Not. R. Astron. Soc. **416**, 3017 (2011).
[73] N. Padmanabhan, X. Xu, D. J. Eisenstein, R. Scalzo, A. J. Cuesta, K. T. Mehta, and E. Kazin, Mon. Not. R. Astron. Soc. **427**, 2132 (2012).
[74] L. Anderson *et al.*, Mon. Not. R. Astron. Soc. **427**, 3435 (2012).
[75] O. Farooq, F. R. Madiyar, S. Crandall, and B. Ratra, Astrophys. J. **835**, 26 (2017).
[76] S. Nesseris, G. Pantazis, and L. Perivolaropoulos, Phys. Rev. D **96**, 023542 (2017).
[77] S. Basilakos, Mon. Not. R. Astron. Soc. **449**, 2151 (2015).
[78] A. Mehrabi, M. Malekjani, and F. Pace, Astrophys. Space Sci. **356**, 129 (2015).
[79] A. Mehrabi, S. Basilakos, and F. Pace, Mon. Not. R. Astron. Soc. **452**, 2930 (2015).